Manufacturing Cycle-Time Optimization Using Gaussian Drying Model for Inkjet-Printed Electronics

Tsun-Ming Tseng[1], Meng Lian[1], Mengchu Li[1],
Philipp Rinklin[2], Leroy Grob[2], Bernhard Wolfrum[2] and Ulf Schlichtmann[1]
{tsun-ming.tseng, m.lian, mengchu.li, philipp.rinklin, leroy.grob, bernhard.wolfrum, ulf.schlichtmann}@tum.de
[1]Chair of Electronic Design Automation, Technical University of Munich, Arcisstraße 21, 80333 München, Germany
[2]Neuroelectronics, Munich School of Bioengineering, Technical University of Munich, Boltzmannstraße 11, 85748 Garching, Germany

***Abstract*—Inkjet-printed electronics have attracted considerable attention for low-cost mass production. To avoid undesired device behavior due to accidental ink merging and redistribution, high-density designs can benefit from layering and drying in batches. The overall manufacturing cycle-time, however, now becomes dominated by the cumulative drying time of these individual layers. The state-of-the-art approach decomposes the whole design, arranges the modified objects in different layers, and minimizes the number of layers. Fewer layers imply a reduction in the number of printing iterations and thus a higher manufacturing efficiency. Nevertheless, printing objects with significantly different drying dynamics in the same layer leads to a reduction of manufacturing efficiency, since the longest drying object in a given layer dominates the time required for this layer to dry. Consequently, an accurate estimation of the individual layers' drying time is indispensable to minimize the manufacturing cycle-time. To this end, we propose the first *Gaussian drying model* to evaluate the local evaporation rate in the drying process. Specifically, we estimate the drying time depending on the number, area, and distribution of the objects in a given layer. Finally, we minimize the total drying time by assigning to-be-printed objects to different layers with mixed-integer-linear programming (MILP) methods. Experimental results demonstrate that our Gaussian drying model closely approximates the actual drying process. In particular, comparing the non-optimized fabrication to the optimized results demonstrates that our method is able to reduce the drying time by 39%.**

***Index Terms*—Inkjet printing, Gaussian drying model, MILP, Layer assignment**

I. Introduction

Over the past decades, printing-based manufacturing has gained increasing focus as an additive fabrication approach for electronic devices [1]. Compared to classical techniques, printing-based fabrication has a higher compatibility with flexible and stretchable materials [2]. Additionally, a variety of materials can be used as substrates. In particular, low-cost substrates can significantly reduce the production cost of electronics compared to classical silicon substrates. For instance, the fabrication of electronic components on cheap substrates such as paper has previously been demonstrated by [3]. Considering these benefits, remarkable efforts have been devoted to pushing the limits of printing-based fabrication. For example, direct inkjet printing of nanoscale gaps below $100\,\mathrm{nm}$ is made possible without any high-resolution lithography [4]. Generally, ensuring error-free print results, enhancing resolution, and increasing manufacturing speed are major challenges in the process.

Inkjet printing is a deposition technique that builds up images and structures in a droplet-by-droplet fashion [5]. During the manufacturing process, *undesired merging of features* and *accidental ink redistribution* can lead to device failure or otherwise unexpected outcomes. Consequently, the drying process is a vital component of the fabrication to ensure error-free print results. In addition, decreasing the ink drying time can be used to effectively shorten the manufacturing cycle-time.

The pressure differences within the features with a single curved geometry may cause the ink to protrude from its original shape. This phenomenon often occurs when printing thin leads and electrodes. Specifically, if closely spaced parallel electrode lines are printed simultaneously, two adjacent lines may merge at the points where the ink protrudes. This undesired merging results in short-cuts in the layout and eventual loss of functionality.

As for the accidental ink redistribution, it can be observed when small (on the order of individual droplets) and large features are printed within the same object [6]. In this case, smaller and larger features exhibit different average surface curvatures. According to the *Young-Laplace equation*, this difference in curvature causes a local increase in pressure in the smaller feature leading to a redistribution of ink material. Following the landing of ink droplets, this unexpected ink redistribution results in the final dried film being thinner in smaller features, leading to a local increase in the sheet resistance of the final structure. Consequently, the final device's functionality and behavior can be negatively impacted.

Aiming towards avoiding the undesired merging of features, [7] develops an approach that ensures the full drying of one of the electrode lines before printing another neighboring line. The lateral spacing between two printed electrode fingers is precisely controlled to $1\,\mu\mathrm{m}$ without any surface modification or substrate patterning. Nevertheless, if the ink or substrate system allows only moderate temperatures, evaporation rates

ICCAD 2021, DOI: 10.1109/ICCAD51958.2021.9643438
https://ieeexplore.ieee.org/document/9643438
https://dl.acm.org/doi/abs/10.1109/ICCAD51958.2021.9643438

are expected to be low causing an increase of the ink drying time. As a result, the manufacturing cycle-time is increased, leading to lower throughput.

Further, [6] develops an algorithm to prevent both the undesired merging of features and accidental ink redistribution. In the following, we will refer to the above-mentioned sites of likely failure as conflicts. This approach detects possible conflicts automatically and decomposes the corresponding features. The problem of conflicts is then modeled as a layer assignment problem and resolved using mixed-integer-linear programming (MILP). Using this approach, features with potential conflicts will be assigned to different layers to avoid merging or ink redistribution. This is because the printed objects are dried in batches and the fabrication artifacts considered in this context only appear in liquid films. In this way, the method finally achieves the desired print outcome. To mitigate the effect of this approach on the overall manufacturing speed, [6] minimizes the number of layers in order to reduce the number of printing iterations. However, as a consequence of layering and drying in batches, the overall manufacturing cycle-time now becomes dominated by the cumulative drying time of these individual layers.

Considering the drying process during manufacturing, the local solvent concentration in the gas phase plays an important role. Spatially varying solvent concentrations in the gas phase lead to corresponding changes in the evaporation rate and thus affect the drying time at a given position. Further, the local solvent concentration in the gas phase after printing a given layer depends on the number, area, and distribution of objects in said layer. Given a fixed number of layers, multiple conflict-free solutions can be found, each resulting in a completely different ink drying time. Therefore, estimating the total drying time of a given layer assignment is essential to decrease the overall manufacturing cycle-time.

This work aims to expand the applicability and benefits of electronic design automation techniques to the manufacturing of inkjet-printed electronics. We propose the first *Gaussian drying model* to evaluate the local evaporation rate in the drying process to yield an accurate estimation of the individual layer's drying time. Based on the Gaussian drying model, we introduce the concept of *drying score* to approximate the actual drying time. As with the local solvent concentration in the gas phase, the drying score of each layer depends on the number, area, and distribution of to-be-printed objects belonging to that layer.

To obtain an optimal layer assignment, we develop an MILP method to minimize the total drying score based on the outcomes of the layer number minimization. Finally, we fabricate a functional design consisting of electronic components. To evaluate the proposed method, we print this exemplary design using the optimized and non-optimized layering results. Comparing the non-optimized fabrication to the optimized result demonstrates that our method decreases the manufacturing cycle-time significantly. Meanwhile, we assess the relationship between the drying score and the actual drying time by using a linear regression model. The analysis implies that the drying score is positively and linearly correlated to the actual drying time. In other words, our Gaussian drying model closely approximates the actual drying process. We assume that our method is generally applicable to the manufacturing of inkjet-printed electronics in a range of materials and production environments.

II. Gaussian drying model

In general, the drying process takes place between the initial deposition of the ink on the substrate and any final curing or fixing. At the interface between the liquid ink and the gas phase, the local evaporation rate is governed by a thermodynamic equilibrium. This equilibrium is formed between the ink's solvent in its condensed, liquid form and the corresponding gaseous state. Two of the most influential parameters on the state of this equilibrium are temperature and the local solvent concentration in the gas phase. Specifically, the more solvent molecules can be found in the gas phase, the slower the evaporation of further molecules will be. Consequently, the overall drying time increases. Macroscopically, variations in the density of objects in a given layer lead to different concentration fields in the gas phase above the print. Therefore, we conclude that the drying time depends on the number, area, and distribution of objects in a given layer.

Our model of the drying process of inkjet-printed electronics is based on the *diffusion-advection equation*, which is used to quantify the transport of dilute species in a fluid. Further, we assume the gas phase in the direct vicinity of the substrate to be well approximated as quiescent and thus ignore advective transport. Consequently, our model reduces to a classic diffusion problem.

In this context, we use the time-dependent solution of the diffusion equation for a finite number of molecules starting in a single position, a Gaussian function with temporally increasing standard deviation [8]. Further, we make use of the linearity and homogeneity of the diffusion equation and superpose a number of point sources to form a new solution [9]. In this paper, we add up the contribution of every point in the layer to approximate the solvent concentration field in the gas phase above the print. Based on these assumptions, we build a function that takes the number, area, and distribution of objects in the layer as parameters to construct our Gaussian drying model.

III. State of the art: Layer number minimization

Our work aims to improve the manufacturing efficiency of inkjet-printed electronics by minimizing the required total drying time for a given design. In particular, to prevent fabrication artifacts, we adopt the MILP method in [6] to achieve conflict-free outputs with the minimum number of layers.

[6] defined two layout features that are likely to cause the merging of objects and the redistribution of ink: the *Laplace* and the *proximity* conflict. The Laplace conflict describes an undesired ink redistribution between two contacting objects

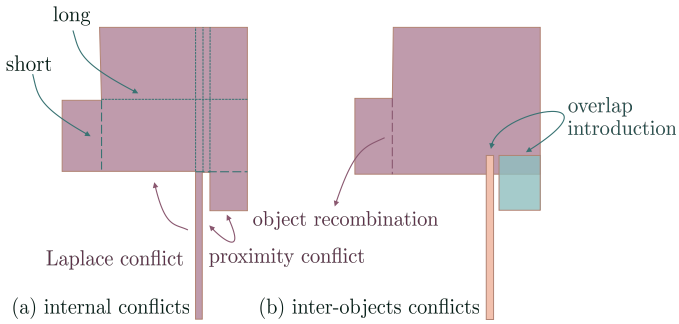

Fig. 1. Illustration of conflicts and decomposition method. (a) The Laplace conflict and proximity conflict can only be observed in the concave vertices. (b) After the decomposition, the conflict-free pairs of objects will be recombined. To ensure proper contact between conflicting polygons, an overlap is introduced.

that differ significantly in their dimensions. As for the proximity conflict, it corresponds to the potential merging of inks when two printed features are located closely together. An example of the two conflicts is shown in Fig. 1 (a).

To resolve the conflicts and thus prevent fabrication artifacts, [6] printed the object in separate layers. Specifically, each object in a conflicting pair was printed only after the previously printed pattern had completely dried. Meanwhile, [6] modeled this problem as a layer assignment problem and developed a method to assign the conflicting features to different layers.

A. Conflict-based object modification

While layering resolves conflicts that occur between different objects, *internal conflicts*, i.e. conflicts within the same object, cannot be eliminated directly by layer assignment. To this end, [6] decomposed objects with internal conflicts into small portions and printed them in distinct layers. In other words, through the decomposition, internal conflicts are transformed into *inter-objects conflicts*, i.e. conflicts between objects, and resolved by layering.

By analyzing the Laplace and the proximity conflict, [6] concluded that internal conflicts can only appear within concave polygons, i.e. polygons with at least one interior angle $>180°$. Therefore, [6] splits all internal angles $>180°$ by extending the adjacent edges of the polygon and selecting the shorter option for decomposition (refer to Fig. 1 (a)). Consequently, all interior angles of the decomposed polygons are $\leq 180°$. Thereafter, the Laplace and proximity conflicts are detected between each pair of decomposed polygons, and the conflict-free pairs are recombined to reduce the number of polygons and thus the computational burden of the subsequent procedure. Moreover, an overlap between contacting and conflicting objects is introduced to ensure proper contact when printed in separate layers (refer to Fig. 1 (b)).

B. Layer assignment for conflict eliminination

After decomposition and recombination, the following constraints are introduced to ensure a correct relative printing order for eliminating all inter-objects conflicts. For each pair of objects that have the Laplace conflict, the smaller object needs to be printed earlier than the larger object. Therefore,

$$l_i + 1 \leq l_j, \tag{1}$$

where l_i and l_j refer to the layer indices of the smaller and the larger objects, respectively. Further, two objects, P_i and P_j, that exhibit a proximity conflict, are not allowed to be printed in the same layer by defining the constraint

$$l_i \neq l_j, \tag{2}$$

where l_i and l_j refer to P_i's and P_j's layer indices, respectively. To apply the constraint (2) in MILP, we first restate it as

$$(l_i + 1 \leq l_j) \vee (l_j + 1 \leq l_i), \tag{3}$$

i.e. either P_i is printed earlier than P_j or P_j is printed earlier than P_i. By using the "big M method", the above constraint is linearized as

$$l_i + 1 \leq l_j + \mathcal{M} \cdot q, \tag{4}$$

$$l_j + 1 \leq l_i + \mathcal{M} \cdot (1 - q), \tag{5}$$

where $\mathcal{M}$ and q represent a very large constant and an auxiliary variable, respectively [10].

Finally, to reduce the number of printing iterations, the objective function is set to minimize the total number of layers, denoted by l_{tot}. To this end, the last constraint is introduced

$$l_i \leq l_{tot}, \tag{6}$$

and the overall problem is modeled as

minimize: l_{tot}

Subject to: (1) and (4) – (6).

IV. Drying Score Minimization

In this paper, we aim to achieve the optimal layer assignment with the minimum total drying time for a given design. The optimization starts from the minimized layer number, i.e. with l_{tot} fixed to its minimum value.

As mentioned in Section II, the drying time of a given layer is dependent on the number of solvent molecules in the gas phase immediately above the print. Generally, within a given layer, the more solvent molecules there are, i.e. the greater the solvent concentration in the gas phase is, the slower the evaporation rate and therefore the longer the drying time will be. Moreover, the highest local solvent concentration in the gas phase of one wet point dominates the solvent concentration in the gas phase of the layer. Consequently, determining the drying time of a layer is equivalent to estimating the highest local solvent concentration in the gas phase of any wet point in that layer. In other words, the drying time of a given layer is equivalent to the longest drying time of any wet points within the layer.

According to our Gaussian drying model, we introduce an indicator of the initial solvent concentration in the gas phase for a given layer. The concept of "initial" refers to the first moment after the ink drop hits the substrate. Specifically, this

TABLE I
MODEL NOTATIONS, CONSTANTS & VARIABLES

Notation	
P_i	The i^{th} object;
$T_{m,n}$	The individual tile on the m^{th} row and n^{th} column;
$P_i^{T_{m,n}}$	The portion of the object P_i in the tile $T_{m,n}$;
Constants	
l_{tot}	The total number of layers;
n_x, n_y	The number of individual tiles in the x- and y-axis;
$f_{\alpha,\mu,\sigma}(\cdot)$	The Gaussian function $f_{\alpha,\mu,\sigma} = \alpha \exp\left(-\frac{(\cdot-\mu)^2}{2\sigma^2}\right)$;
$\delta_{P_i}^{T_{m,n}}$	The occupancy ratio of the i^{th} object in the tile $T_{m,n}$
$\varrho_{P_i}^{T_{m,n}}$	The drying score increase of the tile $T_{m,n}$ caused by the object P_i;
Binary	
q_i^k	The i^{th} object is assigned to the k^{th} layer;
Integer	
l_i	The layer index of the i^{th} object;
Continuous	
$\varrho_k^{T_{m,n}}$	The drying score of the tile $T_{m,n}$ in the k^{th} layer;
ϱ_k	The highest drying score in the k^{th} layer.

indicator is referred to as the drying score and is expected to be proportional to the accurate drying time. To minimize the total drying time of a given design, we minimize the total drying score, which is the sum of each layer's drying score. Thereafter, the layer assignment with the minimum total drying score is the expected optimal solution.

Our approach consists of *area tiling*, *determining the drying score of an individual tile*, and *mathematical model construction*, each of which will be explained in the following. The model notations, constants and variables are outlined in Table I.

A. Area tiling

To physically represent a point, we decompose the entire design into $n_x \times n_y$ square tiles. A larger number of tiles implies a smaller tile making the model more accurate, but also increasing the calculation volume. Thus, this is a tradeoff between accuracy and computational effort. The tile side-length will then be determined according to the entire design size.

According to the area tiling, we obtain for each object the occupancy ratio in each tile by computing the ratio of the *area of the object* to the *area of its located tile*. For example, the

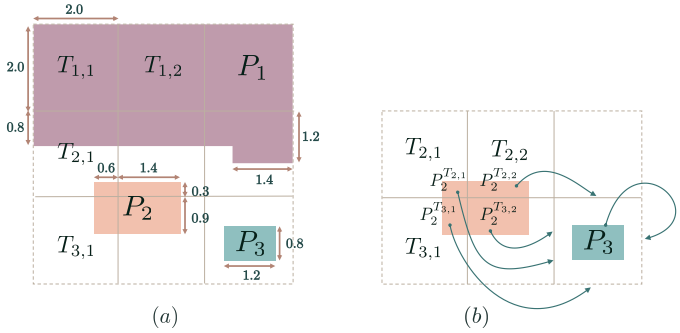

Fig. 2. Illustration of tile occupancy and the drying score increase. (a) A design decomposed into 3×3 square tiles, on which there are three objects: P_1, P_2, and P_3. (b) Ignoring the object P_1 from (a), the drying score of the tile $T_{3,3}$ is determined by summing up the drying score increase caused by P_3 in $T_{3,3}$ and all portions of P_2 in four neighbouring tiles.

occupancy ratios of P_1, P_2, and P_3 in each tile in Fig. 2 (a) are

$$\begin{aligned}
&\delta_{P_1}^{T_{1,1}} = 1.000; \quad \delta_{P_1}^{T_{1,2}} = 1.000; \quad \delta_{P_1}^{T_{1,3}} = 1.000;\\
&\delta_{P_1}^{T_{2,1}} = 0.400; \quad \delta_{P_1}^{T_{2,2}} = 0.400; \quad \delta_{P_1}^{T_{2,3}} = 0.540;\\
&\delta_{P_2}^{T_{2,1}} = 0.045; \quad \delta_{P_2}^{T_{2,2}} = 0.105; \quad \delta_{P_2}^{T_{3,1}} = 0.135;\\
&\delta_{P_2}^{T_{3,2}} = 0.315; \quad \delta_{P_3}^{T_{3,3}} = 0.240,
\end{aligned}$$

and $\delta_{P_i}^{T_{m,n}} = 0$ for the rest m, n, and $i \in \{1, 2, 3\}$.

B. Determining the drying score of an individual tile

To determine the drying score, for each tile containing parts of objects, we build a time-invariant Gaussian function taking the distance from every individual tile to the current one as the argument. Thereafter, the drying score of each tile is calculated by summing up the drying score increase caused by all wet objects in each tile within the layer. In particular, for each tile T, the drying score increase caused by a portion of a wet object located in the tile $\hat{T}$ is the product of the above-mentioned Gaussian function and the occupancy ratio of this object in the tile $\hat{T}$.

Generally, we choose the probability density function of the normal distribution as our Gaussian with the mean set to zero. To demonstrate our example, we set the standard deviation of the Gaussian function as $(n_x + n_y)/8 = 3/4$. Thus,

$$\begin{aligned}
f_{\alpha,\mu,\sigma}(\cdot) &= f_{\frac{1}{\frac{(n_x+n_y)}{8}\sqrt{2\pi}},0,\frac{(n_x+n_y)}{8}}(\cdot)\\
&= \frac{1}{3/4\sqrt{2\pi}} \exp\left(-\frac{(\cdot)^2}{9/8}\right).
\end{aligned} \tag{7}$$

As for the example shown in Fig. 2 (b), the object P_2 will be divided into four parts according to the tiles: $P_2^{T_{2,1}}$, $P_2^{T_{2,2}}$,

and $P_2^{T_{3,1}}$, and $P_2^{T_{3,2}}$. Thereafter, the drying score increase of the tile $T_{3,3}$ caused by P_2 is

$$\begin{aligned}\varrho_{P_2}^{T_{3,3}} &= f_{\alpha,\mu,\sigma}\left(\mathrm{dist}\left(T_{2,1},T_{3,3}\right)\right)\cdot\delta_{P_2}^{T_{2,1}}\\ &+ f_{\alpha,\mu,\sigma}\left(\mathrm{dist}\left(T_{2,2},T_{3,3}\right)\right)\cdot\delta_{P_2}^{T_{2,2}}\\ &+ f_{\alpha,\mu,\sigma}\left(\mathrm{dist}\left(T_{3,1},T_{3,3}\right)\right)\cdot\delta_{P_2}^{T_{3,1}}\\ &+ f_{\alpha,\mu,\sigma}\left(\mathrm{dist}\left(T_{3,2},T_{3,3}\right)\right)\cdot\delta_{P_2}^{T_{3,2}},\end{aligned} \tag{8}$$

where

$$\mathrm{dist}\left(T_{m_1,n_1},T_{m_2,n_2}\right)=\sqrt{\left(m_1-m_2\right)^2+\left(n_1-n_2\right)^2}, \tag{9}$$

denotes the distance between the tile T_{m_1,n_1} and T_{m_2,n_2}. Similarly, the drying score increase of the tile $T_{3,3}$ caused by P_3 is

$$\varrho_{P_3}^{T_{3,3}} = f_{\alpha,\mu,\sigma}\left(\mathrm{dist}\left(T_{3,3},T_{3,3}\right)\right)\cdot\delta_{P_3}^{T_{3,3}}. \tag{10}$$

We substitute equation (7) into equation (8) and equation (10), then obtain

$$\begin{aligned}\varrho_{P_2}^{T_{3,3}} &= f_{\alpha,\mu,\sigma}\left(\sqrt{(2-3)^2+(1-3)^2}\right)\cdot 0.045\\ &+ f_{\alpha,\mu,\sigma}\left(\sqrt{(2-3)^2+(2-3)^2}\right)\cdot 0.105\\ &+ f_{\alpha,\mu,\sigma}\left(\sqrt{(3-3)^2+(1-3)^2}\right)\cdot 0.135\\ &+ f_{\alpha,\mu,\sigma}\left(\sqrt{(3-3)^2+(2-3)^2}\right)\cdot 0.315\\ &= 0.080656,\end{aligned} \tag{11}$$

and

$$\begin{aligned}\varrho_{P_3}^{T_{3,3}} &= f_{\alpha,\mu,\sigma}\left(\sqrt{(3-3)^2+(3-3)^2}\right)\cdot 0.240\\ &= 0.127662.\end{aligned} \tag{12}$$

Finally, the drying score of the tile $T_{3,3}$ is described as

$$\varrho^{T_{3,3}} = \varrho_{P_2}^{T_{3,3}} + \varrho_{P_3}^{T_{3,3}} = 0.208318. \tag{13}$$

C. Mathematical model construction

Our method is based on the minimized layer number, i.e. l_{tot} is fixed to its minimum value as a constant. According to constraint (6), we conclude that each object's layer index is bounded by l_{tot}. Thereafter, we define a binary variable q_i^k for each object and for each layer to denote whether the i^{th} object is assigned to the k^{th} layer. To guarantee that each object is exactly assigned to one layer, the following constraint should be satisfied.

$$\sum_{k=1}^{l_{tot}} q_i^k = 1. \tag{14}$$

To represent the layer index of each object using the above-defined binary variable, we introduce the following equation.

$$l_i = \sum_{k=1}^{l_{tot}} k\cdot q_i^k, \tag{15}$$

where l_i denotes the layer index of the i^{th} object.

As introduced in Table I, the drying score of each tile for each layer is denoted by $\varrho_k^{T_{m,n}}$, where k is the layer index and $T_{m,n}$ is the tile index. $\varrho_k^{T_{m,n}}$ can then be detemined by adding up the drying score increase caused by all the to-be-printed objects within this layer

$$\varrho_k^{T_{m,n}} = \sum_i \varrho_{P_i}^{T_{m,n}}\cdot q_i^k. \tag{16}$$

Since the drying score of each layer is dominated by the maximum drying score among all the tiles, for each tile, we introduce the following constraint.

$$\varrho_k \geq \varrho_k^{T_{m,n}}, \tag{17}$$

where ϱ_k is an auxiliary continuous variable to denote the maximum drying score in the k^{th} layer among all the tiles. Consequently, to minimize the total drying score of a given layout, we minimize the summation of the maximum drying score among the tiles for each layer. The complete optimization problem can therefore be modeled as

$$\begin{aligned}&\textit{minimize: } \sum_{k=1}^{l_{tot}} \varrho_k\\ &\textit{Subject to: (1), (4) – (6), and (14) – (17)}\end{aligned}$$

V. Experimental Result

In this section, we investigate the performance of our Gaussian drying model and our MILP method with six functional layout designs as test cases. Our work was implemented using C++ and the experiments were performed using a computer with a 2.67 GHz CPU. The MILP model is solved by Gurobi [11].

Test cases 1–3 are three basic functional designs, case 4 is a microheater, and case 5 is an experimental design proposed in [6]. In particular, we fabricated a $75\,\mathrm{mm}\times 50\,\mathrm{mm}$ digital microfluidic from [12] as case 6, which contains interdigitated driving electrode array, reservoir electrodes, and contact pads for interfacing with the control system. All printing experiments were performed using a commercial silver nanoparticle ink (DGP 40LT-15C, Sigma-Aldrich), Teonex Q65HA (Dupont Teijin) as a substrate, and disposable cartridges (1 pL DMC, Fujifilm Dimatix) on a Ceradrop F-series printer (Ceradrop). During all prints, the nozzles were kept at 50°C and the chuck was maintained at a temperature of 55°C. The decomposed patterns were processed using the printer's software and printed in individual layers using a drop pitch of $20\,\mu\mathrm{m}$ for rasterization and a jetting frequency of 2 kHz. Upon print completion, the drying state of the patterns was visually inspected in intervals of $\geq$5 min, where the intervals were shortened the more dry the prints appeared. Once the print was fully dry, the subsequent layer was printed and the procedure was continued until all layers of the design were printed. In addition, considering the difficulty of measuring the different deposition times of the layout portions, the drying time of each layer was measured as the time interval between

TABLE II
RESULT COMPARISON FOR OPTIMIZED AND NON-OPTIMIZED LAYER ASSIGNMENTS

Case	#Objects	#Feasible	Optimized	Minimum	Reduction (Minimum)	Median	Reduction (Median)	Maximum	Reduction (Maximum)
1	18	195	6.3979	6.3979	0	7.4323	13.92%	8.3181	23.08%
2	12	5	5.8570	5.8570	0	6.0705	3.52%	6.4916	9.78%
3	16	13	6.4775	6.4775	0	6.8217	5.05%	6.9042	6.18%
4	52	3	23.0382	23.0382	0	23.0382	0	23.0382	0
5	22	3	30.7726	30.7726	0	30.7726	0	30.7726	0
6	710	1000	17.8081	24.9408	28.60%	33.9106	47.49%	34.4650	48.33%

the termination of printing and the moment when the current layer's patterns were completely dry.

As mentioned in section III, to prevent the Laplace and the proximity conflict, the whole design was decomposed and the modified objects were assigned into different layers. We first performed the methods in [6] to obtain the minimum number of layers that ensured conflict-free solutions.

Starting from the minimized layer number, we obtained the optimal layer assignment of to-be-printed objects with the minimum total drying score by using our MILP method. To calculate the drying score, we used the normal distribution function provided by the C++ standard library to construct the probability density function of a normally distributed random variable with the mean as zero and standard deviation as $(n_x + n_y)/32$. Specifically, we set the total tile number to the scale of 10^4, and the Gaussian function is defined as

$$f_{\alpha,\mu,\sigma}(\cdot) = \frac{1}{\frac{(n_x+n_y)}{32}\sqrt{2\pi}} \exp\left(-\frac{(\cdot)^2}{2\left(\frac{(n_x+n_y)}{32}\right)^2}\right),$$

where n_x and n_y are computed as in Section IV-A.

Besides, we randomly generated one thousand different layer assignments based on the corresponding minimum number of layers for each experimental design. In the following, we denote a layer assignment with the minimized layer number as *feasible* when each of its layers is conflict-free. These one thousand layer assignments are referred to as the no-treatment control group for the respective experimental design. Further, layer assignments with the *minimum*, *median*, and *maximum* drying scores in the no-treatment control group are regarded as non-optimized solutions. For convenience, the non-optimized layer assignment with the minimum, median, and maximum total drying score will be referred to as the minimum, median, and maximum non-optimized layer assignment, respectively.

Noticeably, considering the scale of experimental designs, the number of feasible layer assignments may be less than one thousand. If this situation occurs, all feasible solutions will be used to construct the no-treatment control group for that experimental design. The total drying score of the optimal solution and representative non-optimized solutions, as well as the corresponding percentage reductions, are shown in Table II. For each case, we denote the number of to-be-printed objects as #objects and the number of feasible layer assignments as #feasible.

TABLE III
THE DRYING SCORE AND THE ACTUAL DRYING TIMES OF OPTIMIZED AND MEDIAN NON-OPTIMIZED LAYER ASSIGNMENTS

Layer no.	Optimized			Median non-optimized		
	Drying time	Drying score	Time / Score	Drying time	Drying score	Time / Score
1	70	1.3759	50.88	80	1.7109	46.76
2	60	1.2516	47.94	185	6.3744	29.02
3	60	1.1529	52.04	190	6.4736	29.35
4	205	6.2619	32.74	235	6.5331	35.97
5	50	1.0904	45.85	215	6.1939	34.71
6	235	6.6754	35.20	210	6.6247	31.70
	∑Time	**∑Score**	**∑ Time / ∑ Score**	**∑Time**	**∑Score**	**∑ Time / ∑ Score**
	680	**17.8081**	**38.18**	**1115**	**33.9106**	**32.88**

A. Optimized versus non-optimized layer assignments

As mentioned above, we randomly construct for each design one thousand layer assignments as control group. Except for case 6, the number of feasible layer assignments for all other test cases is less than one thousand. Comparing case 1 with case 4, we noticed that the number of decomposed objects in case 1 is 18 and in case 4 is 52. However, there are 195 feasible layer assignments for case 1, while only three for case 4. As a conclusion, the number of feasible solutions is not related directly to the number of to-be-printed objects.

For case 4 and case 5, we observe that the total drying score of their three different feasible layer assignments are the same. Due to the lack of sufficient feasible solutions, there is no difference between optimal and non-optimized solutions. In other words, the optimization simply ensures that the desired outcome can be achieved with minimum printing iterations. While for case 6, there is a significant difference in the total drying score between the minimum and

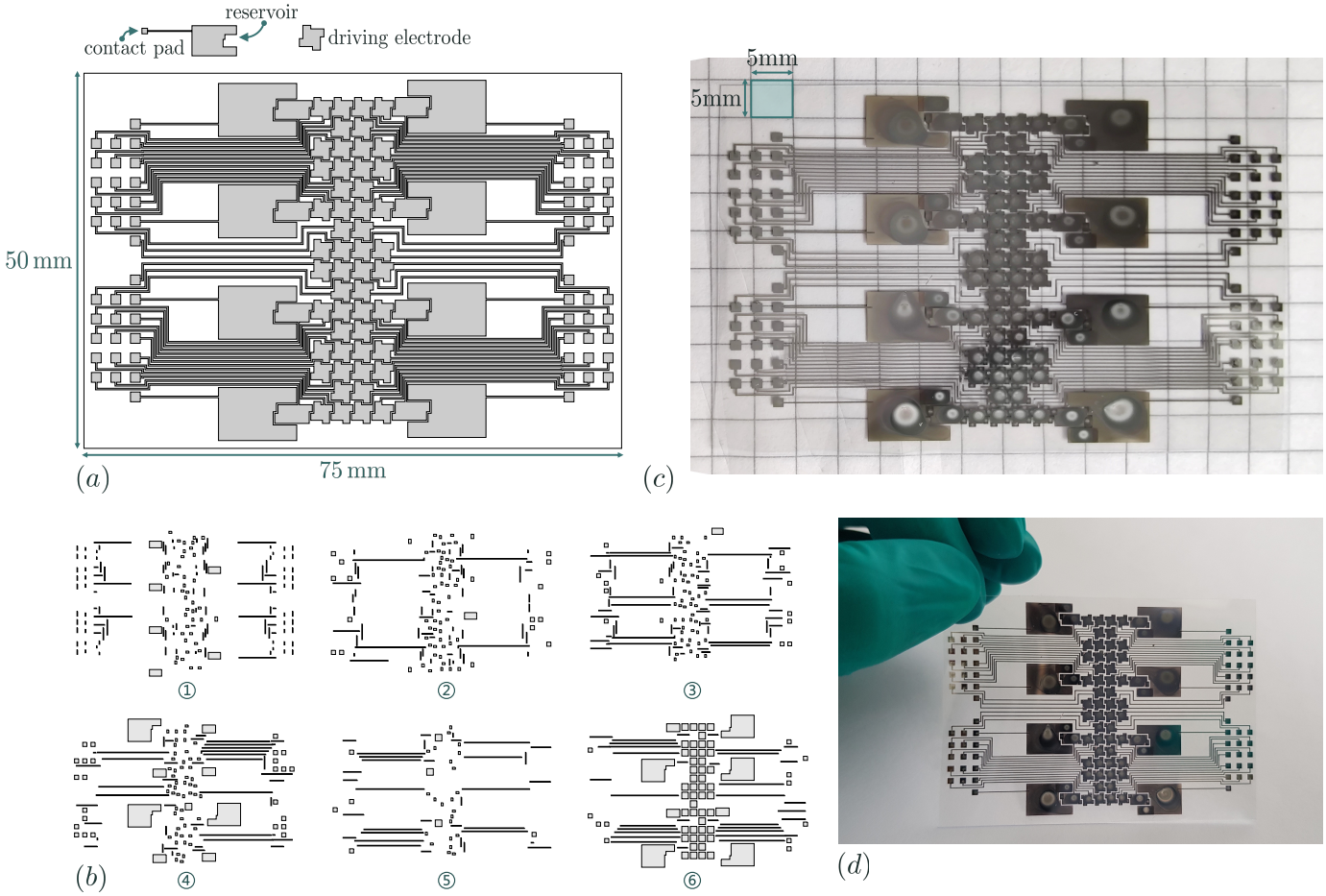

Fig. 3. Case 6: (a) The top-view schematic of substrate. (b) The top-view schematics of each layer for the optimized layer assignment. (c) Image of the optimized design with a grid size of $5\,\mathrm{mm}\times5\,\mathrm{mm}$. (d) Picture of the optimized design printed on the polyester film held by hand.

maximum non-optimized layer assignments, which indicates that there is much space for optimization. Specifically, for case 6 the percentage reduction is 28.60%, 47.49%, and 48.33% comparing the optimized to the minimum, median, and maximum non-optimized layer assignment, respectively. Therefore, the advantage of our method is more significant in designs with a large number of feasible solutions.

Further, we demonstrate in Table III a comparison between the drying score for each layer of the optimized result and median non-optimized layer assignment for case 6. The minimized layer number of case 6 is six. As shown in Table II, the percentage reduction regarding the median non-optimized layer assignment is 47.49%. As for the drying score of each layer, within the optimized solution, only two layers have a drying score greater than six, while within the non-optimized layer assignment five layers have a drying score greater than six (refer to Table III). Comparing the optimal assignments of to-be-printed objects in each layer in Fig. 3 (a), the above-mentioned observation is developed by the fact that the reservoirs in the design shown in Fig. 3 (a) will always dominate the drying score of the layer that they belong to.

Specifically, there is a significant difference between the area of the reservoirs and all other components, which leads to significantly different drying dynamics. Therefore, printing objects with strongly differing drying dynamics in the same layer leads to a reduction in manufacturing efficiency. Noticeably, in the optimized layer assignment shown in Fig. 3 (b), all the reservoirs are divided into two groups and assigned to the fourth and sixth layers to minimize the difference in drying dynamics within one layer.

Meanwhile, considering Table III in conjunction with Fig. 3 (b), we also observe that there is little difference in the drying scores between the fourth and sixth layer, although the sixth layer has one more reservoir than the fourth. This occurs because the drying score depends not only on the number of objects in a given layer but also on the area and distribution of objects contained therein.

B. Gaussian drying model evaluation

To verify our above-mentioned inference, we evaluate the Gaussian drying model by comparing the drying score with the actual drying time of each layer in the optimized layer assignment and in the median non-optimized layer assignment of case 6.

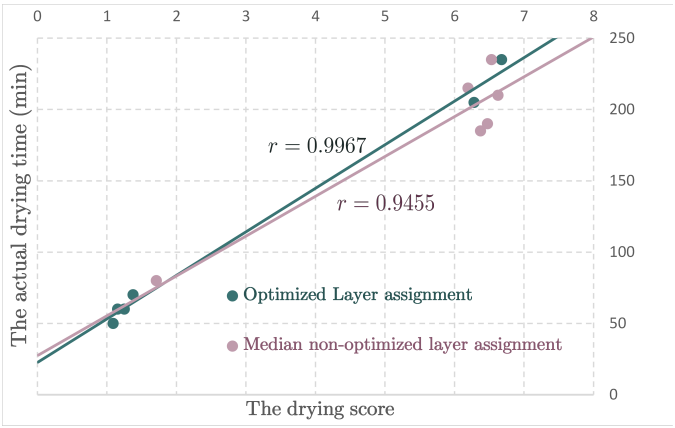

Fig. 4. Illustration of scatterplots and linear regression lines.

In Table III, we exhibit the actual drying time (in minutes) of each layer for the optimized and median non-optimized layer assignments. Generally, we conclude that the drying score is proportional to the actual drying time. For further evaluation, we relate the drying score and actual drying time by using a linear regression model. Specifically, in Fig. 4, we demonstrate the scatterplots and corresponding linear regression lines of the drying score and actual drying time both in the optimized and median non-optimized layer assignments. The x- and y-axes correspond to the drying score and actual drying time, respectively. According to the scatterplots, we conclude that there is a positive correlation between the drying score and actual drying time.

In particular, we introduce the Pearson correlation coefficient r for both layer assignments. In regression, the Pearson correlation coefficient is a measure of linear correlation between two sets of data. $r = 1$ implies that a linear equation describes the relationship between X and Y perfectly, with all data points lying on a line for which Y increases as X increases. As shown in Fig. 4, the Pearson correlation coefficient is 0.9967 in optimized layer assignment and 0.9455 in median optimized layer assignment. We infer that our Gaussian drying model closely approximates the actual drying process as both values are very close to 1.

VI. Conclusion

In this paper, we propose an MILP method to improve the manufacturing efficiency of inkjet-printed electronics by optimizing the printing order of objects in a given design. To estimate the actual drying time for the purpose of reducing manufacturing cycle-time, we construct the first Gaussian drying model and introduce a formula to generate the drying score of a given layer. Thereafter, the optimal solution is obtained by minimizing the total drying score of a given design. Experimental results confirm that our Gaussian drying model closely approximates the actual drying process and the proposed MILP method can significantly reduce the manufacturing cycle-time.

References

[1] V. Subramanian, J. B. Chang, A. de la Fuente Vornbrock, D. C. Huang, L. Jagannathan, F. Liao, B. Mattis, S. Molesa, D. R. Redinger, D. Soltman, S. K. Volkman, and Qintao Zhang, "Printed electronics for low-cost electronic systems: Technology status and application development," in *ESSCIRC 2008 - 34th European Solid-State Circuits Conference*, Sep. 2008, pp. 17–24.

[2] B. G. Levi, "New printing technologies raise hopes for cheap plastic electronics," *Physics Today*, vol. 54, no. 2, pp. 20–22, 2001. [Online]. Available: https://doi.org/10.1063/1.1359701

[3] J. Lessing, A. C. Glavan, S. B. Walker, C. Keplinger, J. A. Lewis, and G. M. Whitesides, "Inkjet printing of conductive inks with high lateral resolution on omniphobic "rf paper" for paper-based electronics and mems," *Advanced Materials*, vol. 26, no. 27, pp. 4677–4682, 2014.

[4] C. W. Sele, T. von Werne, R. H. Friend, and H. Sirringhaus, "Lithography-free, self-aligned inkjet printing with sub-hundred-nanometer resolution," *Advanced Materials*, vol. 17, no. 8, pp. 997–1001, 2021/04/23 2005.

[5] V. Beedasy and P. J. Smith, "Printed electronics as prepared by inkjet printing," *Materials (Basel, Switzerland)*, vol. 13, no. 3, p. 704, 02 2020. [Online]. Available: https://pubmed.ncbi.nlm.nih.gov/32033206

[6] P. Rinklin, T.-M. Tseng, C. Liu, M. Li, K. Terkan, L. Grob, N. Adly, S. Zips, L. Weiß, U. Schlichtmann, and B. Wolfrum, "Electronic design automation for increased robustness in inkjet-printed electronics," vol. 4, no. 4, p. 045002, 2019. [Online]. Available: http://dx.doi.org/10.1088/2058-8585/ab4c1c

[7] N. Adly, L. Feng, K. J. Krause, D. Mayer, A. Yakushenko, A. Offenhäusser, and B. Wolfrum, "Flexible microgap electrodes by direct inkjet printing for biosensing application," *Advanced Biosystems*, vol. 1, no. 3, p. 1600016, 2017.

[8] G. S. Chirikjian, *Gaussian Distributions and the Heat Equation*. Boston: Birkhäuser Boston, 2009, pp. 31–61.

[9] J. F. Cariñena, J. Grabowski, and G. Marmo, "Superposition rules, lie theorem, and partial differential equations," *Reports on Mathematical Physics*, vol. 60, no. 2, pp. 237–258, 2007.

[10] S. Bradley, A. Hax, A. Hax, and T. Magnanti, *Applied Mathematical Programming*. Addison-Wesley Publishing Company, 1977.

[11] G. Optimization, *Gurobi Optimizer Reference Manual*, http://www.gurobi.com.

[12] C. Dixon, A. H. C. Ng, R. Fobel, M. B. Miltenburg, and A. R. Wheeler, "An inkjet printed, roll-coated digital microfluidic device for inexpensive, miniaturized diagnostic assays," *Lab Chip*, vol. 16, pp. 4560–4568, 2016. [Online]. Available: http://dx.doi.org/10.1039/C6LC01064D